



Velocity Structure in an Embedded Corrugated Steel Pipe Model

C. Magura

Department of Civil Engineering, University of Manitoba, Winnipeg, Manitoba, Canada

Abstract: This paper describes the velocity structure in a 0.62m diameter circular corrugated steel pipe with 10% gravel embedment and a projecting inlet, under three slopes (0, 0.5 and 1.0%) and sub-critical flow conditions with discharges ranging from 64 to 254 L/s. Velocity readings were made using a robotically controlled Acoustic Doppler Velocimeter allowing near full flow conditions to be investigated. Two dimensional interpolation was utilized to develop full isovel patterns for 13 cross sections along the 14m length of the model, revealing regions of reduced velocity adjacent to the gravel bed and suggesting strong secondary currents. The logarithmic portion of the central and non-central velocity profiles was examined, revealing a consistent distribution to the Nikuradse equivalent sand roughness and shear velocity around the wetted perimeter. These results have implications relating to culvert design in regions where changes to fish passage criteria have outpaced design theory.

1. Background

Circular corrugated structural plate (CSP) culverts are the most common form of stream crossing on small rivers in Manitoba due to their relatively low cost and ease of installation. However, they are also considered the least desirable form of stream crossing from a fish passage perspective because they inevitably concentrate the flow, resulting in higher velocities than would occur in the natural channel (Canadian Department of Fisheries and Oceans and Manitoba Natural Resources, 1996). If the velocity in a culvert exceeds a certain level, it may act as a barrier to fish attempting to ascend upstream. Flow velocities can be reduced by increasing culvert size, roughness, burial depth, and by reducing culvert slope. Therefore, in an effort to control flow velocities in circular CSP culverts, federal law requires that they be embedded by 0.3 m or 10% of their diameter (whichever is greater) and filled with a suitably graded rock to the level of the natural stream bed. They must also be sized so that fish desiring to proceed upstream do not experience a delay greater than 3 days, once every 10 years. In addition, Manitoba regulations require a flow depth of no greater than half the culvert diameters during periods of fish migration, typically during the spring freshet.

Assuming the hydrology of a river is known accurately, the two key elements to achieving an economical design for a culvert stream crossing are knowledge of the velocity distribution within the culvert and accurate data on the swimming abilities and behaviour of affected fish species. It is well understood that low velocity zones exist near the flow boundaries that may be used by fish traveling upstream. Unfortunately, no methods currently exist to accurately predict the effect of embedment on the velocity distribution in circular culverts under open channel flow conditions. As well, little research has been done to examine the effect of embedment on composite roughness in circular CSP culverts, adding further uncertainty to velocity prediction efforts. As a result, current fish passage models are based on average velocity and may be overly conservative.

Further research is required to bridge the knowledge gap surrounding both prediction of velocity distributions and fish behavioural science with regard to fish passage considerations. In an effort to address the former, this report details a physical modeling study conducted to investigate the flow characteristics of an embedded circular CSP culvert under a range of flows and slopes.

2. Experimental Set-up and Testing

Construction and testing of the model was conducted at the Hydraulics Research and Testing Facility of the University of Manitoba. Water was supplied to the model from a constant head tank capable of delivering a constant discharge of up to $0.485 \text{ m}^3/\text{s}$. Model discharge was measured with a sharp crested weir in the headwater box, calibrated using two volumetric tanks set below the head tank. The model culvert was constructed of a 14.28 m long by 0.62 m diameter (D_o) corrugated metal pipe and was intended to be a 5:1 scale reproduction of a 3 m diameter prototype culvert with 10% embedment. Sampling holes were cut in the obvert at 26 evenly spaced locations along the culvert. The gravel bed consisted of a graded river-wash modeled on Class 350 rip-rap used in culverts in Manitoba (Manitoba Infrastructure and Transportation, 2003). Class 350 rip-rap has a specified particle size distribution of $d_{15} = 100 \text{ mm}$, $d_{50} = 200 \text{ mm}$ and $d_{100} = 350 \text{ mm}$. Undistorted Froudian scaling was applied and the model was constructed with a projecting end inlet as this is the most commonly used inlet configuration in Manitoba. The model consisted of three major components; a headwater box, the culvert, and a tailwater box. The layout and components of the model are shown in Figure 1.

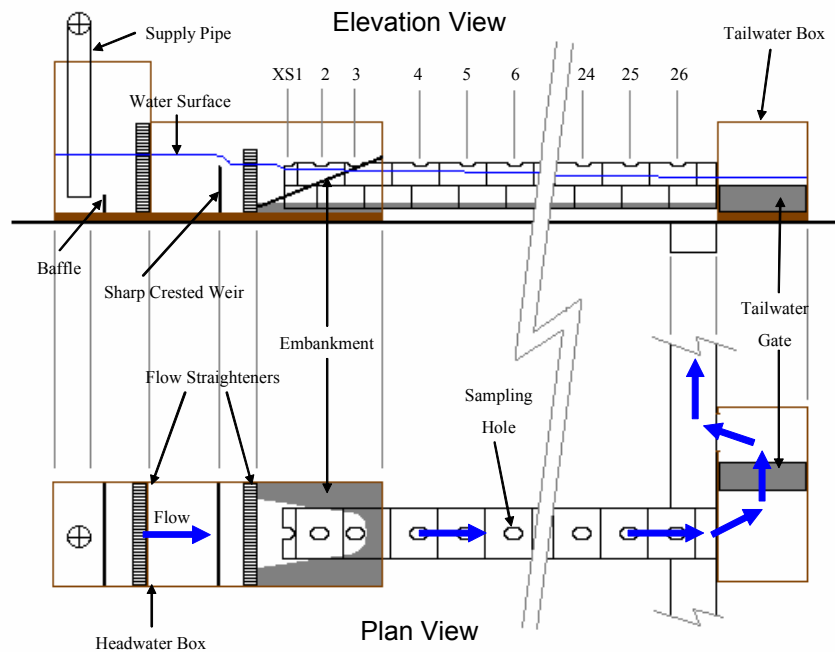


Figure 1: Model layout and components (not to scale).

A dense sampling grid was used for each cross-section with 60 to 120 sampling locations depending upon flow depth (y_o). With each sample requiring 40 seconds, manual sampling of a single cross-section could take several hours. Therefore, an automated sampling system was devised to take the detailed velocity measurements necessary and provide consistency and repeatability of sampling between cross sections. The system components are detailed in Figure 2. Galil's SmartTERM software was used to control the two servo-motors and a polar coordinate sampling system was developed to allow sampling of the entire cross-section through the openings in the culvert obvert. The size of the sampling holes allowed a relative depth of $0.938y/D_o$, the depth at which maximum discharge occurs in a circular culvert.

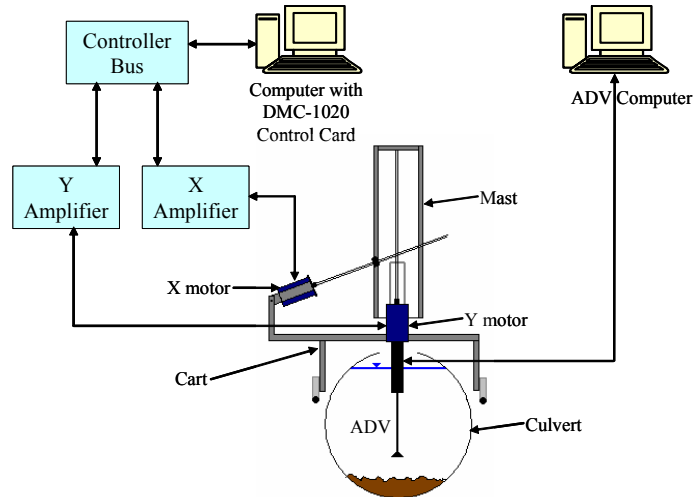


Figure 2: Schematic of the automated sampling system

A downward looking ADV was used and the automated sampling system was used to conduct detailed sampling of flow velocities along the full length of the model under roughly uniform flow conditions. As shown in Table 1, experimental testing was conducted with slopes of 0%, 0.5% and 1.0% and with flows ranging from 0.064 m³/s to 0.254 m³/s, with subcritical flow conditions occurring in all cases. Each slope was tested with a low and high flow case producing a range of average relative depths from 0.42D_o to 0.76D_o. Detailed velocity measurements were made at 13 sampling locations along the length of the culvert (cross-sections 1, 2, 3, 4, 6, 8, 10, 12, 14, 17, 20, 23 and 26) and water surface profiles were recorded for each experimental run, with and without tailwater control.

Table 1: Detailed velocity measurement testing parameters

Slope	Flow (m ³ /s)	Code	Average Depth (m)	Average Froude #
0%	0.064	S0Q64	0.299	0.235
0%	0.186	S0Q186	0.472	0.291
0.5%	0.145	S5Q145	0.305	0.514
0.5%	0.221	S5Q221	0.449	0.387
1.0%	0.150	S1Q150	0.260	0.700
1.0%	0.254	S1Q254	0.386	0.517

3. Analysis Approach

This study places a heavy reliance upon the ability to estimate the velocity at any point within the region of the cross-section where point velocity measurements were taken. Checks performed to assess the validity of this approach showed good agreement between measured and interpolated data. In addition, a continuity check using area-integration of the modeled cross-sections produced good agreement between measured and calculated flow with errors ranging from -6.9% to 0% along the culvert barrel. Due to satisfactory results, extrapolated data is used in a qualitative way to make observations about the velocity structure. It should be noted that parameters such as shear velocity and equivalent sand roughness were calculated using interpolated data from within the sampling region only. The polar coordinate sampling grid used created non-uniformly spaced data points in each cross-section. A two dimensional interpolation of this data was performed using Matlab to create a uniformly spaced matrix of point velocity values, thus filling in the flow area of the cross-section. From each interpolated cross-section, 11 vertical velocity profiles were extracted at $z = 0$ m, $z = \pm 0.06$ m, $z = \pm 0.12$ m, $z = \pm 0.18$ m, $z = \pm 0.24$ m and $z = \pm 0.27$ m, where z equals the lateral distance from the central plane.

4. Velocity Structure

Matlab was used to plot isovels for each cross-section where detailed velocity measurements were taken. Using the interpolated velocity data, 11 vertical velocity profiles were extracted at each cross-section. For ease of viewing, isovel velocities are given in cm/s with increments of 10 cm/s. Color coding of the isovels is consistent for all plots. The vertical velocity profiles are used primarily for determination of shear velocity and equivalent sand roughness but they also provide a level of detail not resolvable from the isovel plots. This additional information was useful in assessing such details as boundary layer growth and the location of the maximum velocity within the cross-section.

Generally, all plots showed good symmetry even close to the inlet. This suggests that the addition of a rough gravel bed may encourage flow symmetry, considering open channel flow is notoriously asymmetrical, even in circular pipes under carefully controlled laboratory experiments (Chow, 1959). Knight and Sterling (2000) presented symmetric isovels resulting from a series of experiments using a circular pipe with a flat bed under open channel flow conditions. However, the symmetry of the isovels they present is perfect to the smallest detail, suggesting that velocity measurements were taken from only half of the cross-section and symmetry was assumed.

4.1 Entrance Region

The isovels for the first three cross-sections of the 0% slope trials are shown in Figure 3 to Figure 6. The most striking feature of both the low and high flow condition is the contraction effect and flow separation associated with it. Having exited the flow straightener only 1 m upstream of the inlet, the flow velocity is nearly uniform through the central portion of the inlet. To pass through the reduced cross-section of the culvert, the flow is forced to accelerate, converting potential energy into kinetic energy in the form of a head loss. The isovels for cross-section 1 reveal that flow first accelerates in the region adjacent to the “dead zone” created by the contraction, forming two nearly symmetrical “velocity pillars”. The velocity

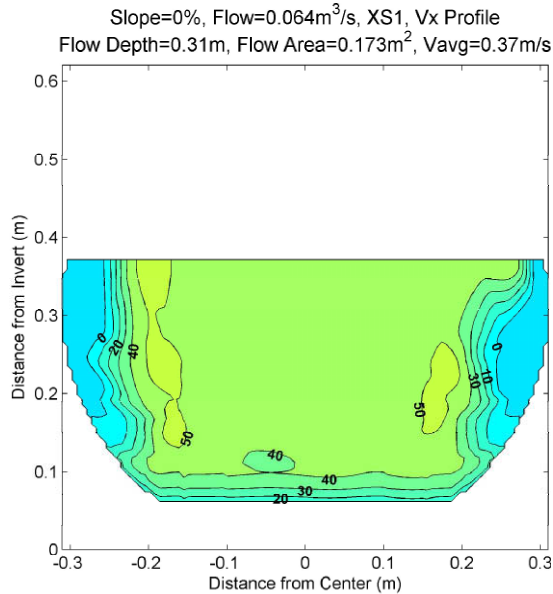


Figure 3: Isovlel Plot for S0Q64 XS1, $y_o=0.310$ m, $A = 0.173 \text{ m}^2$, $u_{avg} = 37.0 \text{ cm/s}$

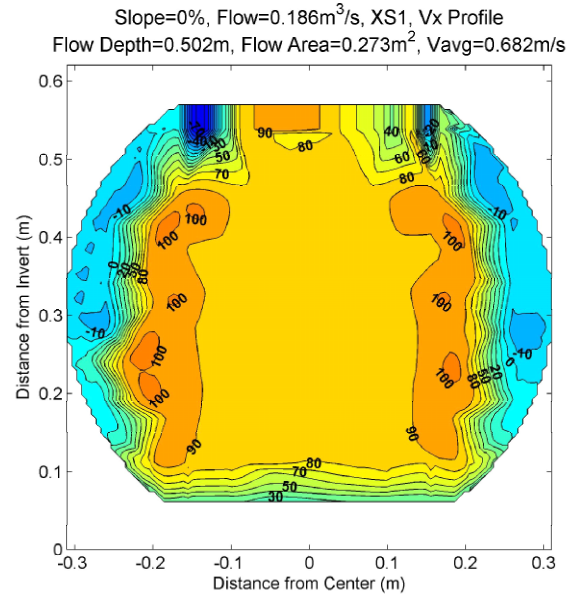


Figure 4: Isovlel Plot for S0Q186 XS1, $y_o=0.502$ m, $A = 0.273 \text{ m}^2$, $u_{avg} = 68.2 \text{ cm/s}$

The extent of the contraction and its effect on the entrance region is consistent with observations of prototype culverts. Behlke et al (1991) state that the flow area through the contraction will be

approximately three-quarters that of the flow area downstream in the barrel for culvert inlets projecting into an inlet pool that is at least twice as wide as the culvert diameter. As the approach channel was almost exactly twice the width of the culvert, this agrees well with the size of the contraction observed in all trials. However, determining the exact location and extent of maximum contraction would have

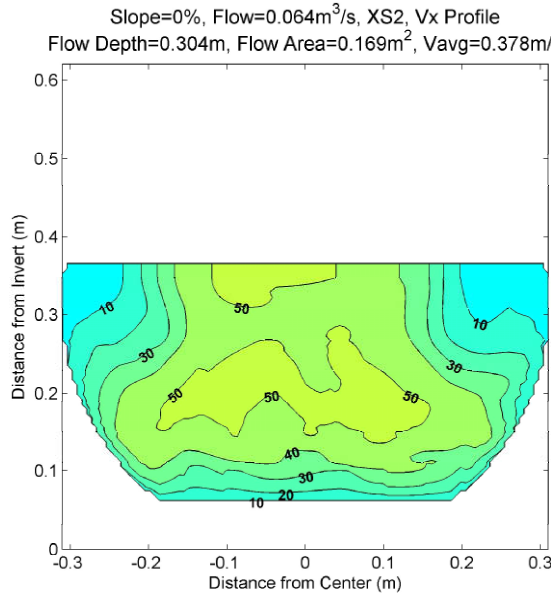


Figure 5: Isovel Plot for S0Q64 XS2, $y_o=0.304$ m, $A = 0.169$ m², $u_{avg} = 37.8$ cm/s

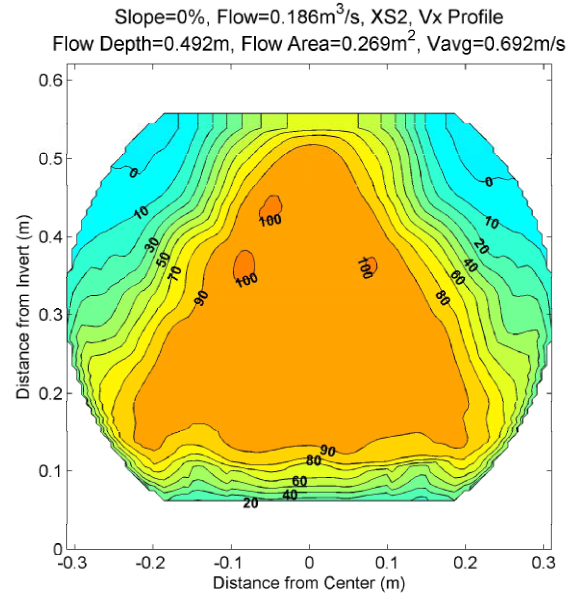


Figure 6: Isovel Plot for S0Q186 XS2, $y_o=0.492$ m, $A = 0.269$ m², $u_{avg} = 69.2$ cm/s

Behlke et al (1991) also mention that while the contraction itself occurs over a very short distance, the deceleration zone after the contraction can persist for several culvert diameters downstream. In all trials, the effect of the contraction was found to disappear by cross-section 4 or 2.6 diameters downstream from the inlet. Once past the contraction, the velocity gradient is reduced near the bed as the bed roughness affects the developing profile. The central portion of the flow becomes almost triangular in shape as the contraction dissipates toward the water surface.

In the eddy of the contraction, mild adverse currents were apparent in all runs. However, surface velocity measurements taken during the 0% slope trials have revealed strong adverse currents in cross-section 1 near the water surface of S0Q186 which are up to 70% of u_{max} in magnitude. These localised eddies are associated with the rapidly varied flow caused by the inlet head losses, which is in turn dependent upon inlet configuration. The sampling density near the water surface is insufficient to fully describe the structure of these localized eddies but does clearly demonstrate the chaotic nature of the flow structure in a projecting inlet under high flow conditions.

4.2 Culvert Barrel

For all runs, the general shape of the isovels has largely stabilised by cross-section 6 (4.4 diameters downstream). Generally, the velocity gradient above the bed is less than that normal to the culvert walls. However, the degree by which they differ varies from run to run. There are three factors that strongly affect the overall shape of the velocity distribution; water depth, velocity, and distance downstream.

4.2.1 Effect of Depth on Isovel Shape

In the low flow cases, where water depth ranged from $0.42y/D_o$ to $0.49 y/D_o$, the isovels are roughly parallel to the cross-section boundaries, forming a nearly convex shape as in Figure 7. The maximum velocity generally occurs in the central plane of the cross-section within a depth of $0.5y/y_o$ to $0.6y/y_o$, where y_o is the average depth of flow. For all three low flow runs, the velocity gradient normal to the

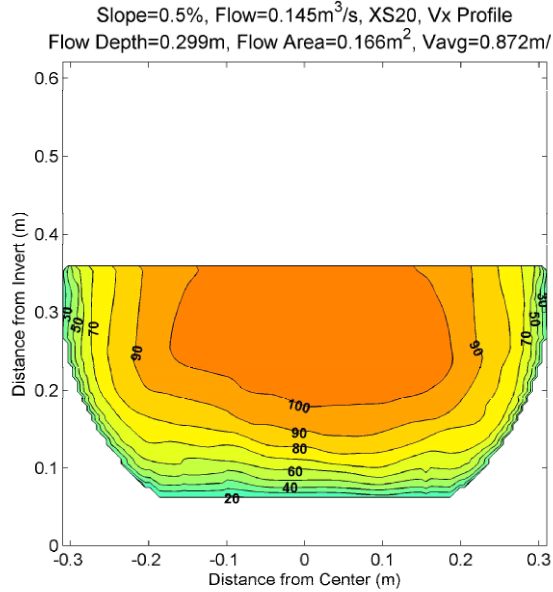


Figure 7: Isovel Plot for S5Q145 XS20, $y_o=0.299$ m, $A=0.166 \text{ m}^2$, $u_{avg}=87.2 \text{ cm/s}$

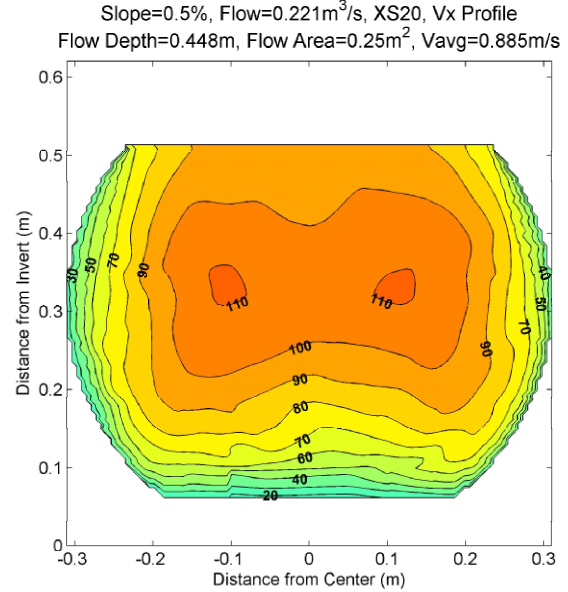


Figure 8: Isovel Plot for S5Q221 XS20, $y_o=0.448$ m, $A=0.250 \text{ m}^2$, $u_{avg}=88.5 \text{ cm/s}$

In the high flow cases, where water depth ranged from $0.62y/D_o$ to $0.76 y/D_o$, the difference in the bed and wall velocity gradient is greatly increased. The isovels veer away from the bed sharply, forming a distinct zone of lower velocity water affected by the bed. This bed-affected region protrudes into the central flow of the culvert, imparting a relatively symmetrical dual-lobed shape upon the isovels as can be clearly seen in Figure 8. For all three high flow cases, the maximum velocity (u_{max}) occurred within a depth of $0.6y/y_o$ to $0.7 y/y_o$. Initially, the u_{max} of S1Q254 occurred at the central plane but by 6 diameters downstream, u_{max} was nearly uniform across half the width of flow. For the S0Q186 and S5Q221 runs, u_{max} occurred in the central plane only in cross-section 4, after which the localized maximum velocity occurred simultaneously at $z = \pm 0.12$ m. For S0Q186, this condition persisted until cross-section 17, or for a distance of 14 diameters downstream. For S5Q221, the dual u_{max} persisted along the full length of the culvert. In both S0Q186 and S5Q221, the velocity profile along the culvert continued to shift toward a more concentric structure as seen in S1Q254

4.2.1 Effect of Velocity on Isovel Shape

As the average velocity of the flow increases, the extent of bed affected region diminishes and the maximum velocity becomes more localized in the center plane. The isovels are parallel to the culvert boundaries in the S0Q64 run along nearly the full length of the culvert, showing a slight dip toward the bed by cross-section 26. This trend occurs sooner and to a greater degree as the average velocity in the low flow cases is increased. In Figure 9 the isovels for S1Q150 can be seen to dip towards the bed, creating a high velocity gradient centered over the bed and diminishing towards the sides. The most extensive zones of low velocity water are near the corner where the bed and wall meet.

This effect has been observed in other studies of circular pipes flowing partly full with a flat bed (Knight and Sterling, 2000). They investigated a wide range of flow and simulated embedment depths. In runs where there was significant embedment and the cross-section became roughly rectangular; Knight and Sterling (2000) observed compression of the isovels in the region of the corners. They attributed this to secondary currents, as described in Schlichting (1979). In their experiments the bed and sidewall of the test pipe had uniform roughness. As the isovels in S1Q150 took on a similar shape to those described by Knight and Sterling's experiments, this may suggest that as the velocity in an embedded culvert increases, the relative effect of the bed roughness on the shape of the isovels decreases, while the effect

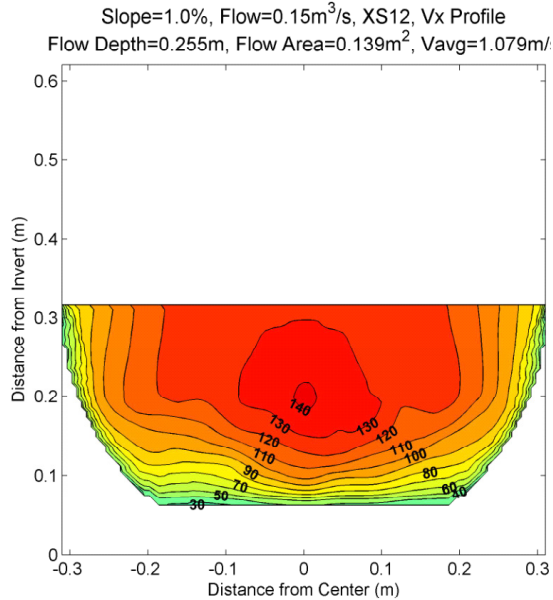


Figure 9: Isovel Plot for S1Q150 XS12, $y_o=0.255$ m, $A=0.139$ m², $u_{avg}=107.9$ cm/s

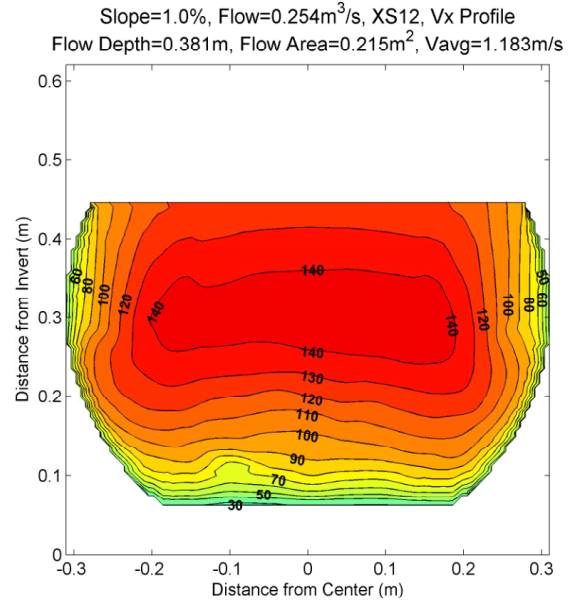


Figure 10: Isovel Plot for S5Q254 XS12, $y_o=0.381$ m, $A=0.215$ m², $u_{avg}=118.3$ cm/s

The isovels for cross-section 12 of S1Q254 are shown in Figure 10. In the high flow cases, the bed affected region becomes less distinct as the average velocity increases. This effect is even more pronounced than in the low flow cases. Also, the isovels in Figure 10 are nearly parallel to the culvert boundaries without the distinctive dual-lobed shape seen in S0Q186 and S5Q221. Consequently, as the velocity increases, the region of highest velocity becomes more localized toward the central plane and more concave in shape.

5. Log Law Region

The vertical velocity profiles extracted from each interpolated flow cross-section were used to determine the shear velocity (u_*) and equivalent sand roughness (k_s) at $z = 0$ m, ± 0.06 m, ± 0.12 m, ± 0.18 m, ± 0.24 m and ± 0.27 m from the central plane. The corresponding non-central velocity profiles (e.g. $z = \pm 0.06$ m) were averaged and the distribution of u_* and k_s was assumed to be symmetrical about the central plane.

5.1 Shear Velocity

For each cross-section the central and averaged velocity profiles were plotted semi-logarithmically and a trend line was fit to the linear portion of each. The slope of these trend lines divided by 2.5 is equivalent to the shear velocity as seen when the Prandtl-von Karman universal-velocity-distribution law is rearranged thus:

$$[1] u = (2.5u_*') \ln \frac{y}{k_s} + 8.5$$

The results from cross-section 1 to 4 were found to be highly erratic, owing to the inlet disturbance and the contraction effect. For this reason, only the results from cross-section 6 to 26 are reported. For each run, the shear velocity was found to vary consistently with distance from the central plane and the curves collapse significantly when normalized by the global shear velocity for each run as shown in Figure 11. Global shear velocity is calculated as

$$[2] u_{*o} = \sqrt{gRS_f}, \text{ where } g \text{ is acceleration due to gravity, } R \text{ is hydraulic radius and } S_f \text{ is friction slope.}$$

The shape of the profile is consistent between runs, with u_* increasing with water velocity and the maximum u_* occurring typically between $z = 0.06 \text{ m}$ to 0.12 m . The center plane shear velocity is always somewhat lower than the peak, due to the low velocity zone created by the bed. Toward the culvert wall, the shear velocity drops off significantly, approaching 20 to 50% of the peak, depending upon the run. The relative magnitude of the shear velocity between experimental runs is most strongly related to average velocity but also varies somewhat across the culvert bed. This demonstrates the dependence of shear velocity upon velocity gradient, and therefore isovel shape, which is in turn influenced by water depth, velocity and variation in boundary roughness. The shear velocity showed no significant trend along the length of the culvert allowing the results for cross-sections 6 to 26 to be averaged.

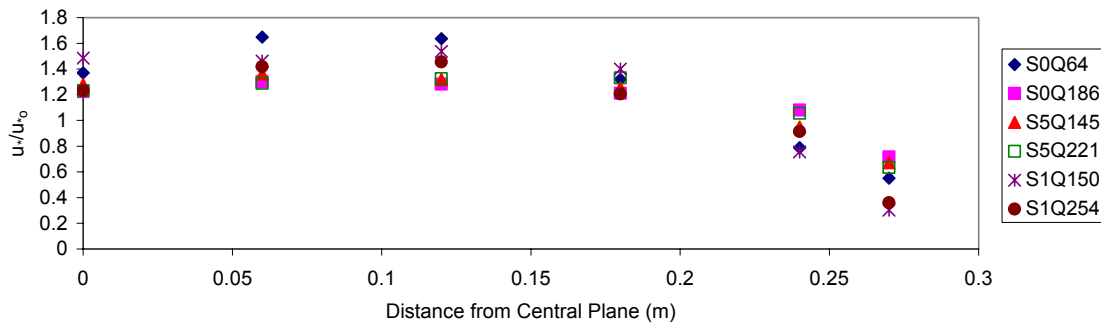


Figure 11: Distribution of shear velocity normalized by global shear velocity (averaged over XS6-26)

5.2 Equivalent Sand Roughness

After calculating the shear velocity at the base of each vertical profile, the velocity profiles were plotted again as u/u_* versus y/k_s and fit to the Prandtl-von Karman universal velocity distribution law. The equivalent sand roughness was determined by adjusting it to align the logarithmic portion of each profile with the Log Law. Like shear velocity, only the results from cross-section 6 to 26 are reported.

Figure 12 shows the value of k_s for each experimental run from $z = 0 \text{ m}$ to 0.27 m . There was significant variation in k_s along the length of the culvert due primarily to the difficulty in accurately determining both the shear velocity and the highly variable surface of the gravel bed, which prevented the distance to the boundary from being determined exactly. However, there was no discernable trend in k_s along the length of the culvert and mean values are reported from cross-section 6 to 26. Over the culvert wall, the average k_s dropped rapidly, approaching a value equivalent to the corrugation height, as previously determined by Ead et al (2000). Numerous methods have been proposed to relate roughness to the grain size of bed material in gravel rivers. For comparison purposes, a value of k_s based on Charlton, Brown and Benson (1978) is also plotted on Figure 12. Charlton et al. (1978) calculate k_s as

$$[3] k_s = 3D_{84} < k_s < 3D_{90}$$

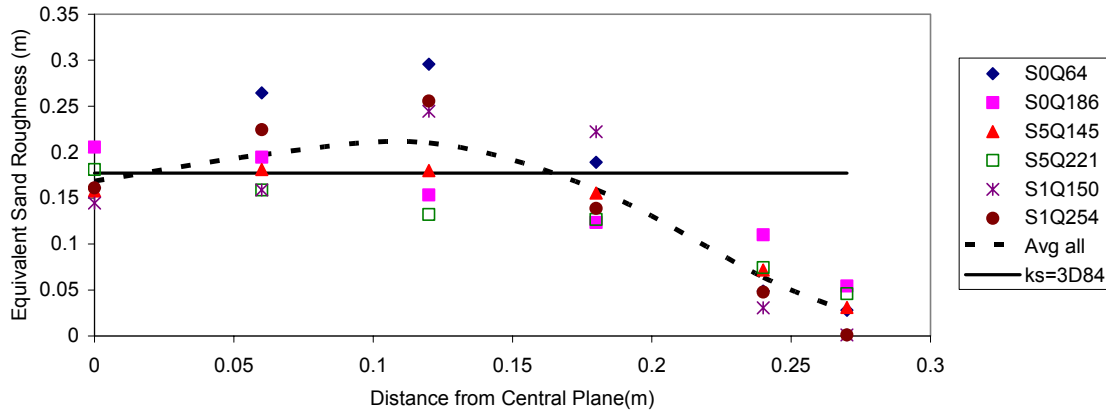


Figure 12: Distribution of equivalent sand roughness (averaged over XS6-26)

6. Discussion and Recommendations

Experimental testing was conducted with slopes of 0%, 0.5% and 1.0% and with flows ranging from 0.064 m³/s to 0.254 m³/s, with subcritical flow conditions occurring in all cases. Each slope was tested with a low and high flow case producing a range of average relative depths from 0.42D_o to 0.76D_o. Detailed velocity measurements were made at 13 sampling locations along the length of the culvert and isovel plots were developed for each run. Examination of the isovel plots and vertical velocity profiles revealed that the velocity structure is strongly influenced by the contraction effect of the inlet, the water depth, and the average velocity. In all experimental runs, a strong contraction effect was measured; reducing the available flow area by 25% immediately downstream from the inlet. Measured velocities within the contraction reached as high as 150% of the average inlet velocity. The contraction effect appeared to dissipate by roughly 3 diameters downstream from the inlet for all runs.

For all flow depths, the velocity gradient normal to the culvert walls was less than the velocity gradient over the gravel bed, though the extent by which they differed varied greatly. At relative flow depths approaching 0.5D_o, the isovel contours are roughly parallel to the culvert bed and walls. At relative depths closer to 0.75D_o, a distinct low velocity zone developed over gravel bed, protruding into the flow towards the center of the culvert and creating a dual-lobed appearance to the isovel structure. Local velocity maxima were observed on both sides of the culvert. As the average flow velocity increased, this bed-affected region of low velocity water became less distinct, with the isovels beginning to dip towards the center of the bed in the low flow runs. These results demonstrate the complex velocity structure occurring within the inlet region and barrel of embedded culverts under open channel flow conditions. The level of complexity in the flow structure presents a significant challenge to developing robust velocity prediction methods.

A number of researchers have observed that in circular CSP culverts, juvenile and weak swimming fish utilize the low velocity zones adjacent to the culvert wall and water surface (Behlke et al., 1991). These zones are often attributed to the presence of secondary currents and tend to become smaller or disappear once the flow depth in the culvert becomes greater than half the diameter. An interesting observation may be made from this relating to fish passage in embedded culverts. The Manitoba Stream Crossing Guidelines for the Protection of Fish and Fish Habitat (DFO and MNR, 1996) state that the flow depth in culverts is not to exceed half the culvert diameter during fish migration periods, presumably to ensure that the low velocity migration zones will be present. However, unless a behavioral or biological basis exists that requires juvenile and weak swimming fish to exclusively use these surface migration zones, then they will also be able to ascend upstream using the low velocity zones created by the rough gravel bed. Hence, the continued relevance of stipulated maximum water depths as part of fish passage criteria should be critically reviewed in light of embedment requirements for culverts.

By cross-section 6, roughly 4.4 diameters downstream from the inlet, the vertical velocity profiles were generally well described by the Log Law up to the maximum velocity and the logarithmic portion of the profiles was used to determine the distribution of shear velocity (u_*) and equivalent sand roughness (k_s) across the width of flow and along the length of the culvert barrel. For each run, significant variation occurred in the distribution of both parameters along the culvert barrel in the region of fully developed flow, more so with k_s than with u_* . This variation is related in part to the difficulty in accurately determining individual shear velocities from velocity profiles. Accurate measurement of k_s across each cross-section was further hindered by the high variability of the gravel bed surface. As no clear trend was observed along the culvert barrel, the results of each run were averaged for the region of fully developed flow and strong trends emerged in the distribution of both parameters across the width of flow.

The shape of the u_* profiles were consistent between runs, and the individual curves collapsed significantly when normalized by global shear velocity (i.e. u_*/u_{*o}). Shear velocity tended to increase with average water velocity, with peak values ranging from $1.28u_{*o}$ to $1.64u_{*o}$ occurring between $z = 0.06$ m to 0.12 m. The center plane shear velocity was always somewhat lower than the peak ($1.23u_{*o}$ to $1.48u_{*o}$), reflecting the low velocity zone created by the bed. Toward the culvert wall, the shear velocity dropped off significantly, approaching $0.2u_{*o}$ to $0.6u_{*o}$, depending upon the run. The trend in k_s was similar, though more variable between experimental runs, as mentioned above. The k_s value averaged across all runs was close to the predicted range of $3D_{84}$ to $3D_{90}$ across most of the gravel bed. Over the culvert wall, the average k_s dropped rapidly, approaching a value equivalent to the corrugation height. The trends demonstrated herein suggest that u_* and k_s may have a predictable distribution related to flow parameters and boundary roughness. An understanding of the distribution of these parameters may have applications in the development of a robust velocity prediction model.

7. Acknowledgements

I would like to thank my sponsors for their generous support: Manitoba Infrastructure and Transportation, Manitoba Hydro and Armtec Limited. I would also like to thank the following people for their support and advice: Dr. Jay Doering, Ron Richardson, Tim Lock, Ninel Gonzalez and Roy Bukowski.

8. References

- Behlke, C.E., Kane, D.L., McLean, R.F., and Travis, M.D. 1991. *Fundamentals of culvert design for passage of weak-swimming fish*. U.S. Department of Transportation, Report No. FHWA-AK-RD-90-10.
- Charlton, F.G., Brown, P.M., and Benson, R.W. 1978. *The hydraulic geometry of some gravel rivers in Britain*. H.R. Wallingford, Report No. IT180.
- Canadian Department of Fisheries and Ocean and Manitoba Natural Resources. 1996. *Manitoba stream crossing guidelines for the protection of fish and fish habitat*. 48 pp. + app.
- Chow, V.T. 1959. *Open-Channel Hydraulics*. McGraw-Hill, New York, N.Y., USA.
- Ead, S.A., Rajaratnam, N., Katopodis, C., and Ade, F. 2000. Turbulent open-channel flow in circular corrugated culverts. *Journal of Hydraulic Engineering*, 126(10). 750-757.
- Knight, D.W., and Sterling, M. 2000. Boundary shear in circular pipes running partially full. *Journal of Hydraulic Engineering*, 126(4). 263-275.
- Manitoba Infrastructure and Transportation. 2003. Specifications for Stone Rip Rap. *Standard Construction Specifications*, No. 1297. July 2003.
- Schlichting, H. 1979. *Boundary Layer Theory*. 7th ed., McGraw-Hill, New York, N.Y., USA.